Draft version January 19, 2006
Preprint typeset using LaTeX style emulateapj v. 6/22/04

RED MERGERS AND THE ASSEMBLY OF MASSIVE ELLIPTICAL GALAXIES: THE FUNDAMENTAL PLANE AND ITS PROJECTIONS

Michael Boylan-Kolchin[1], Chung-Pei Ma[2], and Eliot Quataert[2]

Draft version January 19, 2006

ABSTRACT

Several recent observations suggest that gas-poor (dissipationless) mergers of elliptical galaxies build up the massive end of the red sequence. We perform a series of major merger simulations to investigate the spatial and velocity structure of the remnants of such mergers. Regardless of orbital energy or angular momentum, we find that the stellar remnants lie on the fundamental plane defined by their progenitors, a result of virial equilibrium with a small tilt due to an increasing central dark matter fraction. However, the locations of merger remnants in the projections of the fundamental plane – the Faber-Jackson and $R_e - M_*$ relations – depend strongly on the merger orbit, and the relations steepen significantly from the canonical scalings ($L \propto \sigma_e^4$ and $R_e \propto M_*^{0.6}$) for mergers on radial orbits. This steepening arises because stellar bulges on orbits with lower angular momentum lose less energy via dynamical friction on the dark matter halos than do bulges on orbits with substantial angular momentum. This results in a less tightly bound remnant bulge with a smaller velocity dispersion and a larger effective radius. Our results imply that the projections of the fundamental plane – but not necessarily the plane itself – provide a powerful way of investigating the assembly history of massive elliptical galaxies, including the brightest cluster galaxies at or near the centers of galaxy clusters. We argue that most massive ellipticals are formed by anisotropic merging and that their fundamental plane projections should thus differ noticeably from those of lower mass ellipticals even though they should lie on the same fundamental plane. Current observations are consistent with this conclusion. The steepening in the $L - \sigma_e$ relation for luminous ellipticals may also be reflected in a corresponding steepening in the $M_{\rm BH} - \sigma_e$ relation for massive black holes.

Subject headings: galaxies: elliptical and lenticular, cD — galaxies: evolution — galaxies: formation — galaxies: fundamental parameters

1. INTRODUCTION

Several independent lines of evidence point to the importance of gas-poor (dissipationless) mergers in the assembly of massive elliptical galaxies. For example, the decreasing rotational support and transition from disky to boxy isophotal shapes with increasing stellar mass in elliptical galaxies suggests an increasing fraction of dissipationless mergers in the growth of the most massive elliptical galaxies (e.g., Bender et al. 1992; Kormendy & Bender 1996; Faber et al. 1997; Naab et al. 2005). There is also indirect evidence from the evolution of galaxy luminosity functions (Bell et al. 2004; Faber et al. 2005; Blanton 2005) and semi-analytic models of galaxy formation (Kauffmann & Haehnelt 2000; Khochfar & Burkert 2003b; De Lucia et al. 2005) that a significant fraction of low-redshift ellipticals were assembled via dissipationless mergers. Moreover, there is direct observational evidence for a substantial number of "red" mergers between early-type galaxies in an intermediate redshift galaxy cluster (van Dokkum et al. 1999; Tran et al. 2005) as well as in more local galaxies (Bell et al. 2005; van Dokkum 2005). In spite of the importance of gas-poor mergers, however, the properties of these mergers and their remnants are not fully understood.

If elliptical galaxies gain substantial mass via mostly dissipationless merging at $z \lesssim 1$, this process could have a significant impact on their properties. The purpose of this paper is to study how such mergers affect the global dynamical and kinematic structure of the remnants, as ellipticals show a very tight correlation in the space spanned by their half-light radii (R_e), central velocity dispersions (σ_e), and central surface brightnesses (I_e) known as the fundamental plane (Dressler et al. 1987; Djorgovski & Davis 1987). Relationships between two of the fundamental plane variables, such as the Faber-Jackson relation (Faber & Jackson 1976) and the stellar mass-size relation, may also serve as important constraints for galaxy formation models (e.g., McIntosh et al. 2005).

This is particularly true for the most luminous elliptical galaxies, including brightest cluster galaxies (BCGs) that populate the exponential tails of the galaxy luminosity, mass, and velocity dispersion functions and contain the most massive black holes in the universe. These galaxies are likely to have undergone multiple generations of gas-poor mergers, as repeated merging during cluster formation is a well-motivated mechanism for BCG formation (Merritt 1985; Dubinski 1998). In this model, anisotropic infall along cosmological filaments introduces a preferential direction in the merging process (West 1994), in contrast to mergers of galaxies in less overdense environments. As discussed below, we suspect that this special assembly history has implications for the scaling relations of massive ellipticals: the preferentially radial orbits of mergers that form the most luminous ellipticals may lead to different Faber-Jackson and stellar mass-size

[1] Department of Physics, University of California, Berkeley, CA 94720; mrbk@berkeley.edu
[2] Department of Astronomy, University of California, Berkeley, CA 94720

relations for these galaxies than for normal ellipticals.

There are, in fact, tantalizing observational hints of deviations from the canonical elliptical galaxy scaling relations for BCGs and other luminous ellipticals. For example, Oegerle & Hoessel (1991) find that while BCGs lie on the same fundamental plane as lower mass ellipticals, their central velocity dispersions change very little with increasing luminosity and their effective radii increase steeply with luminosity, significantly more so than for normal ellipticals. A similar effect is present in the early-type galaxy sample of the Nuker team (see fig. 4 of Faber et al. 1997 and Lauer et al. 2006, in prep.), while Wyithe (2005) has claimed to detect an analogous change in the $M_{\rm BH} - \sigma_e$ relation for the most massive black holes.

In this paper, we present the results of a large number of simulations of major mergers of elliptical galaxies. Our galaxy models contain dark matter halos and stellar bulges, both simulated with sufficient force and mass resolution to reliably investigate the remnants down to scales of $\sim 0.1 R_e$ (over 10^6 total particles per simulation). We consider a wide variety of energies and angular momenta for the merger orbits and quantify the effects of orbital parameters on the merger remnants. This work is a significant extension of our earlier related study (Boylan-Kolchin et al. 2005, hereafter BMQ), where we considered only a few possible orbits for the merging galaxies. The simulations presented in this paper allow us to study in detail the effects of dissipationless merging and merger orbits on the fundamental plane and its projections. Section 2 describes the initial galaxy models and simulation parameters. Section 3 contains the results of our simulations, including the locations of merger remnants in the fundamental plane (Section 3.1) and its projections (Section 3.2). In Section 4 we discuss our results and their implications for the assembly of massive elliptical galaxies and their central black holes.

2. METHODS

The galaxy models used in our simulation consist of dark matter halos and stellar spheroids and are fully described in BMQ; we review the essential features here. The initial dark matter halos have the Navarro et al. (1997) density profiles with a virial mass $M_{200} = 10^{12}\, M_\odot$ and a concentration $c = 10$, resulting in a virial radius of 162.6 kpc and scale radius of 16.26 kpc. The initial stellar bulges have the Hernquist (1990) density profiles with a total stellar mass $M_* = 5 \times 10^{10}\, M_\odot$, resulting in a stellar baryon fraction of $f_b = 0.05$. The additional free parameter in the stellar profile, the scale radius a, is set by the $R_e - M_*$ relation measured for SDSS elliptical galaxies by Shen et al. (2003)

$$R_e = 4.16 \left(\frac{M_*}{10^{11}\, M_\odot} \right)^{0.56} \text{ kpc}, \qquad (1)$$

where $R_e = 1.8153\, a$ for the Hernquist profile; this gives $R_e = 2.82$ kpc for our initial models. We include the effects of baryonic dissipation via the adiabatic contraction model of Blumenthal et al. (1986). Although the applicability of adiabatic contraction to elliptical galaxies is not fully obvious, recent hydrodynamic simulations suggest that it is surprisingly accurate (Gnedin et al. 2004). The resulting (circular) aperture velocity dispersion within R_e for the stellar component in our models is $\sigma_e = 151$ km/s. Although we present the parameters of our initial conditions in physical units, we note that the simulations reported here can be readily scaled to other stellar and dark matter masses (see BMQ for details). We also perform a number of unequal mass mergers, with mass ratio 0.33:1, where the less massive galaxy also has $f_b = 0.05$ and a scale radius set by equation (1).

TABLE 1
Summary of Merger Simulations

Run[a]	Mass[b]	Orbit[c]	V_{orb}[d]	r_p[e]	ϵ[f]
P1	1:1	Parabolic	250	0	–
P2	1:1	Parabolic	250	2.29	–
P3	1:1	Parabolic	250	12.5	–
P4	1:1	Parabolic	250	37.8	–
P5	0.33:1	Parabolic	222	0	–
P6	0.33:1	Parabolic	222	2.31	–
P7	0.33:1	Parabolic	222	12.5	–
P8	0.33:1	Parabolic	222	20.5	–
B1	1:1	Bound	200	0	0.00
B2	1:1	Bound	200	2.29	0.10
B3	1:1	Bound	200	20.8	0.30
B4	1:1	Bound	200	37.8	0.40
B5	1:1	Bound	200	57.1	0.48
B6	1:1	Bound	200	78.4	0.56

[a]Name of run
[b]Mass ratio of progenitors
[c]Energy of run (either parabolic or bound)
[d]Initial orbital velocity (km s^{-1}) for a galaxy with $M_{\rm dm} = 10^{12} M_\odot$ and $M_* = 5 \times 10^{10} M_\odot$
[e]Pericentric distance of orbit (kpc)
[f]Circularity of orbit (undefined for parabolic orbits)

We use `GADGET-1` (Springel et al. 2001) to perform the merger simulations. All runs use a force softening of 0.3 kpc ($= 0.106 R_e$) and equal-mass particles for the stellar and dark matter components: $N_* = 2.5 \times 10^4$, $N_{\rm DM} = 5 \times 10^5$ for each galaxy model. The initial particle positions of each component are sampled from the component's spherically symmetric density profile. To ensure that the models are in equilibrium, we compute separate distribution functions for the halo and bulge and then use these distribution functions to initialize the particle velocities, which are assumed to be isotropically distributed. N-body models set up with this procedure are in general extremely stable over many dynamical times (e.g., Kazantzidis et al. 2004), which we have explicitly checked for our models. An additional source of spurious evolution inherent to N-body simulations is two-body relaxation, a consequence of using simulation particles that are many orders of magnitude more massive than the stars or dark matter particles they represent. We have performed test runs to ensure that two-body relaxation does not affect our results for the duration of the simulations (~ 6 Gyr) for our choices of particle number and force resolution (see BMQ for detailed resolution and stability studies).

The halo centers in the merger simulations are initially separated by two virial radii and the orbital parameters are defined in the standard two-body point mass approximation (Binney & Tremaine 1987, Appendix 1D; Khochfar & Burkert 2003a). In this limit, orbits can be characterized by two quantities: energy E and angular momentum L, or equivalently, pericentric distance r_p and

eccentricity e (or circularity $\epsilon \equiv \sqrt{1-e^2}$ for runs with $E < 0$). The orbital parameters for all of our production runs are listed in Table 1. Since our goal is to understand the effects of different orbits on the properties of the merger remnant, we consider both parabolic encounters and bound orbits, and for each energy we perform simulations for a range of orbital angular momentum. The energy of the bound orbits is taken to correspond to the most probable energy from Benson (2005), which is based on a study of dark matter halo mergers averaged over all cosmological environments. We use this value of E only as a rough guide and note that existing statistical studies of dark matter halo mergers are dominated by low mass objects and therefore do not necessarily represent the orbits responsible for the assembly of massive elliptical galaxies in cluster environments. Larger samples of halos should soon provide robust statistical information about the environmental dependence of halo mergers. In particular, as we argue later in this paper, major mergers leading to the formation of central massive galaxies in clusters may follow preferentially radial orbits.

The non-spherical nature of the luminous portion of merger remnants means that quantities such as R_e and σ_e depend on the orientation at which the object is viewed. An immediate consequence is that an intrinsic scatter in the fundamental plane projections will exist solely due to a variation in viewing angle. In order to compute R_e and σ_e that can be compared with observations, and to quantify the effects of viewing angle, we observe the remnant in each simulation from 10^4 different lines of sight chosen randomly from points on a sphere. The effective radius is determined by the radius of the circle containing half of the projected stellar mass and the mass-weighted aperture velocity dispersion is computed within one R_e.

3. RESULTS

3.1. *The Fundamental Plane*

The fundamental plane is typically expressed in the coordinate system defined by the observables $(x, y, z) = (\log \sigma_e, \log I_e, \log R_e)$ as

$$R_e \propto \sigma_e^a I_e^{-b}\,, \quad \text{or} \quad z = ax - by + z_0\,, \tag{2}$$

where a represents the angle of the plane from the vertical axis $z = \log R_e$, and b/a represents the amount of rotation about the z-axis. If we write

$$M_*(< R_e) \equiv c_1\, I_e R_e^2 \quad \text{and} \quad M_{\rm dyn}(< R_e) \equiv c_2\, \frac{\sigma_e^2 R_e}{G}\,, \tag{3}$$

where c_1 and c_2 are structure coefficients, then the fundamental plane observables are related by

$$R_e \propto \frac{c_2}{c_1} \left(\frac{M_{\rm dyn}}{M_*}\right)^{-1} \sigma_e^2 I_e^{-1} \tag{4}$$

(Bender et al. 1992). Therefore, if elliptical galaxies form a homologous sequence (if c_1 and c_2 are constant) with light tracing dynamical mass and a constant stellar mass-to-light ratio, they should lie on the virial plane given by $a = 2$, $b = 1$. However, the observed fundamental plane differs from the virial plane. For example, $a = 1.24 \pm 0.07$, $b = 0.82 \pm 0.02$ in the Gunn r-band (Jorgensen et al. 1996) and $a = 1.53 \pm 0.08$, $b = 0.79 \pm 0.03$ in the K-band (Pahre et al. 1998b). Results for all SDSS wavebands are similar to the K-band fundamental plane (Bernardi et al. 2003a). This difference represents a "tilt" in the observed fundamental plane from the virial plane: assuming $M_* \propto L$, either c_2/c_1 or $M_{\rm dyn}/M_*$ varies systematically with galaxy mass.

Fig. 1 shows the locations of all of our equal-mass merger remnants in the edge-on projection of each of the three planes discussed above – virial, r-band, and K-band. We find that the 0.33:1 merger remnants show all the same trends as the 1:1 remnants and thus the former are not plotted here. The $1-\sigma$ errors of the fundamental plane in the direction of R_e are indicated by the dotted lines in Fig. 1. Each remnant is marked with a different color, and each point represents one random viewing angle of the remnant. The initial galaxy is spherical by construction, so it is located at a single point in the fundamental plane (large triangle; lower-left corner). The stellar mass-to-light ratio has been chosen so that the initial model lies on the observed fundamental plane (this corresponds to K-band and r-band mass-to-light ratios of 1.0 and 3.6, respectively); the same stellar mass-to-light ratios are used to place the merger remnants on the fundamental plane.

The left panel of Fig. 1 shows that all of the remnants lie significantly off the simple virial theorem expectation. Strikingly, however, *all* of the simulated observations of *all* of the merger remnants lie well within the $1-\sigma$ errors of the fundamental plane for both the optical and near-infrared planes. These results establish that the remnants of major mergers of spherical elliptical galaxies lie on the fundamental plane defined by their progenitors for the wide range of orbital energies and angular momenta covered by our simulations. We note, however, that our dynamic range in R_e and M_* is rather modest, and all of our simulations begin at the same point in the fundamental plane. Thus our simulations cover only a limited part of the observed plane.

Since massive elliptical galaxies may have undergone multiple dissipationless mergers during their assembly history, we also performed a simulation in which the two progenitors were randomly chosen to be the remnants of runs P3 and B6 and the orbit was parabolic with $r_p = 21$ kpc. We find this re-merger remnant lies on the same fundamental plane as the initial galaxy model and first-generation merger remnants (Fig. 1, black region in upper right corner). This single re-merger simulation is certainly not definitive, but it does support the hypothesis that the presence of elliptical galaxies on the fundamental plane is consistent with multiple generations of dissipationless merging.

While the observed fundamental plane is typically plotted in the $(x, y, z) = (\log \sigma_e, \log I_e, \log R_e)$ space as shown in Fig. 1, we find it useful to interpret the plane theoretically in the transformed coordinate system $(x', y', z') = (\log M_{\rm dyn}, \log M_*, \log R_e)$, in which a plane can be written as

$$M_{\rm dyn} \propto M_*^{1+\mu} R_e^{\nu}\,, \quad \text{or} \quad z' = \frac{1}{\nu}\,[x' - (1+\mu)y'] + z_0'\,, \tag{5}$$

where both $M_{\rm dyn}$ and M_* refer to the masses enclosed within R_e. The parameters μ and ν quantify how the ratio of dark matter mass to stellar mass within R_e varies with increasing galaxy mass and size.

Comparing equations (2) and (5), and using the defi-

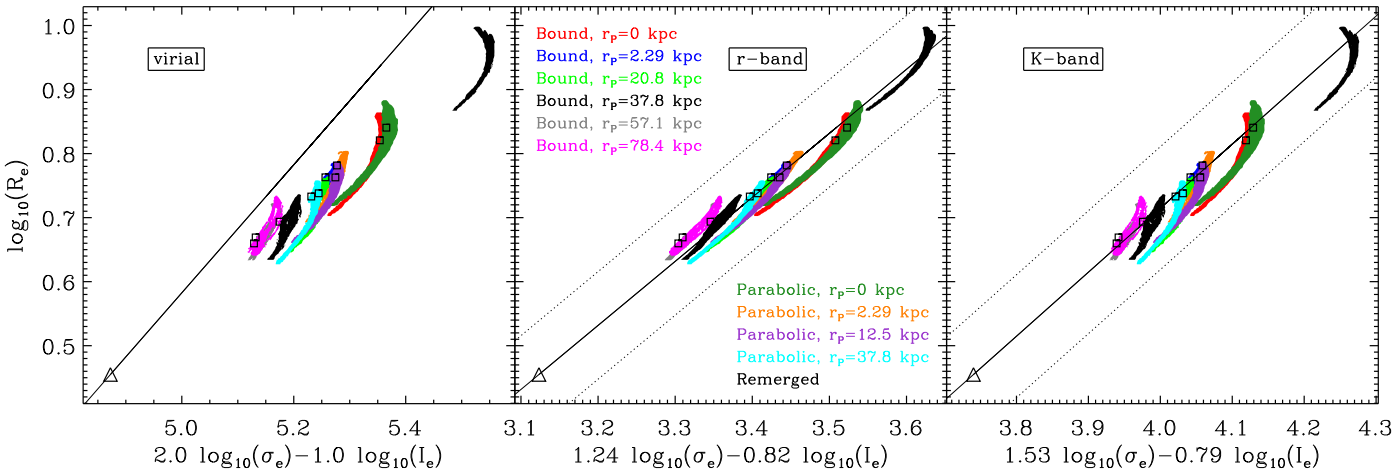

FIG. 1.— Locations of our equal-mass merger remnants in the plane in $(\log\sigma_e, \log I_e, \log R_e)$-space that corresponds to the edge-on projection of the virial plane (left), r-band fundamental plane (middle; Jorgensen et al. 1996), and K-band fundamental plane (right; Pahre et al. 1998b). The solid line in each panel indicates a slope of 1 for the edge-on view; the dotted lines in the middle and right panels indicate the observed $1-\sigma$ scatter in the direction of R_e. For each panel, each simulation (corresponding to a particular energy and angular momentum) is plotted with a different color and each point of a given color corresponds to one of 10^4 viewing angles. A single re-merger simulation, using the remnants of runs P3 and B6 as initial galaxies and with a parabolic orbit with $r_p = 21$ kpc, is plotted in black in the upper right corner as well. For each simulation, squares mark the "most probable" remnant. The initial galaxy model is a single point (large triangle). The effective radii are measured in kpc, the velocity dispersions in km s^{-1}, and surface brightnesses in $10^{10}\,M_\odot\,\mathrm{kpc}^{-2}$ for all panels.

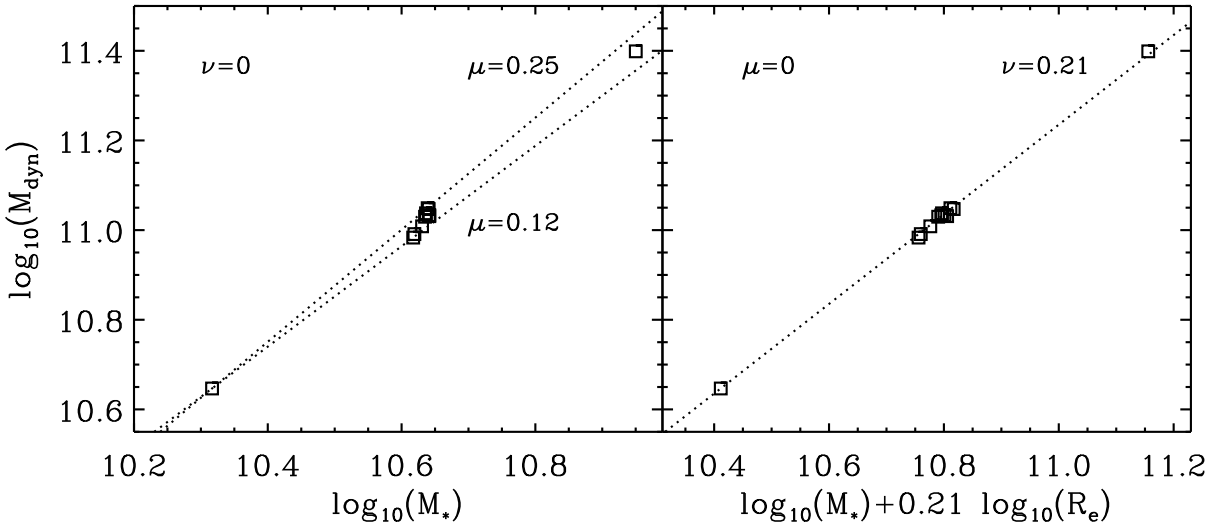

FIG. 2.— Locations of the merger remnants from Fig. 1 in $(\log M_{\rm dyn}, \log M_*, \log R_e)$-space: $M_{\rm dyn} \propto M_*^{1+\mu} R_e^{\nu}$. Both $M_{\rm dyn}$ and M_* are computed within a sphere of radius R_e. *Left:* The $\nu = 0$ plane, which is a good approximation to the r-band plane (fig. 1b). The dotted lines correspond to $M_{\rm dyn} \propto M_*^{1+\mu}$ with $\mu = 0.12$ (lower) and $\mu = 0.25$ (upper); these bracket the results of our simulations. *Right:* The $\mu = 0$ plane, which fits the observed K-band fundamental plane well. We plot the parameterization of the tilt in the fundamental plane that best fits our simulations: $M_{\rm dyn}/M_* \propto R_e^{0.21}$ (dotted line).

nitions in equation (3), gives

$$\mu = \frac{2b}{a} - 1\,, \quad \nu = 1 + \frac{2(1-2b)}{a}\,. \tag{6}$$

The virial plane of $a = 2, b = 1$ corresponds to $\mu = 0, \nu = 0$ (i.e. $M_{\rm dyn} \propto M_*$); it is therefore conveniently parallel to axis $z' = \log R_e$ in the $M_{\rm dyn} - M_* - R_e$ space. The observed r-band and K-band fundamental planes have $(\mu, \nu) = (0.323, -0.0323)$ and $(\mu, \nu) = (0.0327, 0.242)$, respectively. It is interesting to note that the r-band plane of Jorgensen et al. (1996) has $\nu \approx 0$, i.e. $M_{\rm dyn}/M_* \propto M_*^{\mu}$, while the K-band fundamental plane has $\mu \approx 0$, i.e. $M_{\rm dyn}/M_* \propto R_e^{\nu}$.

Fig. 2 shows the locations of our merger remnants in the edge-on view of the $\nu = 0$ (left panel; appropriate for r-band) and $\mu = 0$ (right panel; appropriate for K-band) planes. The remnants appear more consistent with the K-band plane than the r-band plane. Although Fig. 2 and Fig. 1bc display the same information in different

coordinate systems, Fig. 2 illustrates clearly how the dynamical mass within R_e increases more than the stellar mass within the same radius, meaning that the inner regions of our merger remnants are more dark matter-dominated than their progenitors. This increasing dark matter fraction with increasing galaxy mass is the primary cause for the tilt of the observed fundamental plane from the virial plane in our gas-poor mergers.

Since systematic non-homology and varying central dark matter fraction in elliptical galaxies are often considered as possible origins for the tilt of the fundamental plane (e.g., Faber et al. 1987; Ciotti et al. 1996; Pahre et al. 1998a; Gerhard et al. 2001; Padmanabhan et al. 2004; Trujillo et al. 2004), it is useful to assess the importance of non-homology in the context of the two-component dark matter and stellar models considered in this paper. We find that both c_1 and c_2 [as defined in equation (3)] are constant for our merger remnants[3]: $c_1 = 2.70$ with a maximum deviation of $< 4\%$ and $c_2 = 2.90$ with a maximum deviation of $< 3\%$. This implies that the final systems (bulge+halo) are in virial equilibrium and are dynamically homologous (because c_2 is constant) and that the luminous portions of our remnants are structurally homologous (because c_1 is constant). The total system is structurally non-homologous, however, due to a change in the dark matter halo relative to the bulge. The inner part of the halo, which contains the bulge, does not grow as much as the bulge during the course of each merger, while the outer part of the halo expands significantly. This results in an increasing central dark matter fraction for the remnants, as shown in Fig. 2. Since the bulges themselves *are* structurally homologous (c_1 is constant and the density profiles of the remnant bulges are well-fit by a Hernquist profile), we refer to a varying dark matter fraction rather than a structural non-homology.

A further point of interest is that the scatter due to viewing angle variation of the non-spherical remnants in our simulations (represented by the spread within each color in Fig. 1) is roughly parallel to the observed fundamental plane. This trend is a consequence of the virial equilibrium of individual galaxies: at fixed *stellar* mass, $\sigma_e^2 R_e \sim R_e^{0-0.33}$, so $R_e \propto \sigma_e^{-(2-3)}$. Intuitively, a non-spherical remnant maintains a small line-of-sight velocity dispersion by extending in the perpendicular direction. This indicates that while viewing angle variation introduces some scatter into the fundamental plane (González-García & van Albada 2003), this scatter tends to be along the fundamental plane itself. In addition, the scatter due to viewing angle variation does not increase between the first and second generation mergers, further indicating that the fundamental plane scatter is relatively insensitive to dissipationless merger history.

Similar conclusions about mergers and remergers preserving the fundamental plane have been reached in various settings by previous authors (Capelato et al. 1995; Nipoti et al. 2003; González-García & van Albada 2003; Robertson et al. 2005). The previous remerger simulations most relevant to this work are those of Nipoti et al. (2003) and Robertson et al. (2005). They show that both remergers of two-component galaxies similar to ours and remergers of triaxial remnants of gaseous disk galaxy mergers lie on the (K-band) fundamental plane. These results suggest that the spherical symmetry typically assumed in initial galaxy models of merger simulations, albeit unrealistic, does not significantly affect the results on the preservation of the fundamental plane. Exploring the evolution of the fundamental plane under dissipationless merging for general triaxial initial conditions would be useful; however, we believe that a brute-forced sampling of the large parameter space associated with merging triaxial galaxies is highly inefficient. We will discuss a more economical procedure in Section 4 that uses the results of cosmological simulations to motivate realistic merging sequences.

3.2. *Projections of the Fundamental Plane*

The fact that our merger remnants are consistent with the fundamental plane does not necessarily imply that the properties of the remnant are insensitive to the merger orbit, nor does it imply that the remnants necessarily follow the observed Faber-Jackson or $R_e - M_*$ relations: requiring a galaxy of a given mass to lie on the mean of both fundamental plane projections picks out a single point in $R_e - \sigma_e - I_e$ space, whereas the fundamental plane at fixed mass forms a line in the same space (an $R_e - \sigma_e$ correlation).

In order to quantify the effects of merger orbits on the projections of the fundamental plane, we compute the slopes in the $R_e \propto M_*^{\alpha}$ and $M_* \propto \sigma_e^{\beta}$ relations for each of our 1:1 merger simulations. Fig. 3 shows the dependence of the slopes α (left) and β (right) as a function of the pericentric distance of the orbit[4] for both the bound orbits (diamonds) and parabolic orbits (squares). The slopes have a strong trend with pericentric distance: increasing r_p corresponds to decreasing α and decreasing β. These trends were already noted in BMQ based on a few orbits, but the comprehensive set of simulations with different L and E presented in this paper provide a much more quantitative understanding of the impact of the merger orbit on the fundamental plane projections. The slopes for the re-merger remnant, marked with an X in Fig. 3, agree well with those for the first generation mergers. Although Fig. 3 shows only the results of 1:1 merger simulations, we find similar trends in 0.33:1 mergers. These results suggest that the angular momentum and energy of the orbit have the biggest impact on the fundamental plane projections, with the mass ratio of the merging galaxies and the internal structure of the initial bulge/halo system being of secondary importance.

For comparison, the observed fundamental plane projections are $R_e \propto L^{0.56-0.63}$ and $L \propto \sigma_e^{4-4.14}$ (Pahre et al. 1998b; Bernardi et al. 2003b), although as noted in Section 1, these scalings are probably not applicable to the most luminous ellipticals. Our high angular momentum simulations have scaling relations in good agreement with both of the observed projections. The low angular momentum runs, however, deviate significantly from these canonical scalings (similar deviations for low-L runs were also noted in Nipoti et al. 2003,

[3] Note that we compute the surface *mass* density, while it is the surface *luminosity* density that is measured observationally. The two are simply related by the stellar mass-to-light ratio, which we assume is constant.

[4] At fixed energy, varying the angular momentum is equivalent to changing the pericentric distance.

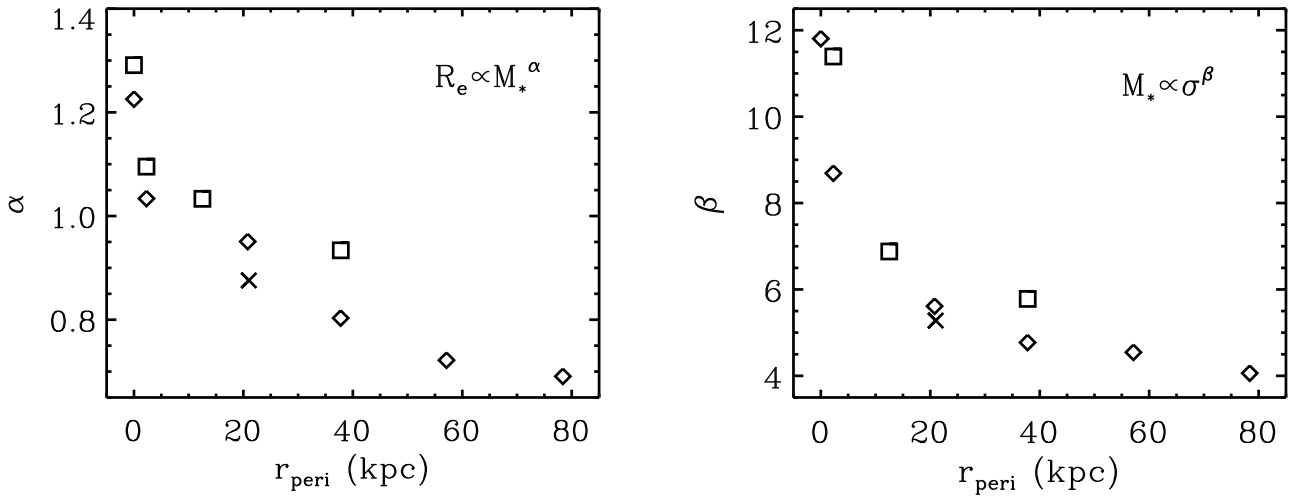

FIG. 3.— Logarithmic slopes of the mass-size relation ($R_e \propto M_*^{\alpha}$; left) and Faber-Jackson ($M_* \propto \sigma_e^{\beta}$; right) relations as a function of orbital pericentric distance for each of the equal-mass merger simulations listed in Table 1. The two orbital energies are shown as diamonds (bound) and squares (parabolic), while the re-merger run is marked with an X symbol. At a given $r_{\rm peri}$, the bound orbits produce remnants with a slightly lower α and β than parabolic orbits. The parabolic head-on orbit has $\beta \approx 28$, so it is not plotted here. For orbits with significant orbital angular momentum (large $r_{\rm peri}$), our merger simulations reproduce the observed values of $\alpha \sim 0.6$ and $\beta \sim 4$ but we predict a sharp increase in α and β for more radial mergers. The results for the re-merger run agree well with those for the first generation mergers, indicating that the spherical and isotropic galaxy models used in the first generation mergers do not strongly bias our results.

BMQ, and Robertson et al. 2005).

The combination of Figs. 1 and 3 reveal that while all of the remnants lie on the fundamental plane, the remnant properties are nonetheless strongly affected by merger orbits. Differences in merger orbits can lead to significant differences in the projected scaling relations but variations in the $R_e - M_*$ relation are compensated by corresponding variations in the $M_* - \sigma_e$ relation, maintaining the fundamental plane because of virial equilibrium of the bulge-halo system.

Qualitatively, the dramatic steepening of the $R_e - M_*$ and $M_* - \sigma_e$ relations with decreasing orbital angular momentum in Fig. 3 can be understood by considering the role of dynamical friction and energy transfer during a merger. At a given orbital energy, stellar bulges with substantial angular momentum need to lose more L (and accordingly, more energy) via dynamical friction on the background dark matter halo than do bulges on low L orbits. This leads to a more tightly bound remnant bulge with a larger σ (smaller β) and smaller R_e (smaller α), as is found in the simulations. The same effect also explains why orbits with more initial orbital energy (our parabolic orbits) tend to lead to less bound remnants with smaller σ (larger β) and larger R_e (larger α).

Quantitatively, we can understand the essence of the physics involved in producing the trends seen in Fig. 3 by examining the energy equation for the stellar bulges. The energy conservation equation for two identical bulges, each with initial stellar mass $M_{*,i}$ and effective radius R_i, merging to form a final bulge of mass $M_{*,f}$ and effective radius R_f can be written as

$$f_f \frac{M_{*,f}^2}{R_f} = 2 f_i \frac{M_{*,i}^2}{R_i} + \eta \frac{M_{*,i}^2}{2R_i}\,. \tag{7}$$

The parameter f depends on the structure of the bulge and surrounding dark matter halo:

$$f \frac{M_*^2}{R_e} \equiv \frac{1}{2} \int \frac{\rho_*(r) M_{\rm dyn}(r)}{r} {\rm d}^3{\rm x}\,, \tag{8}$$

where $M_{\rm dyn}(r) = M_*(r) + M_{dm}(r)$. The parameter $\eta \equiv f_{\rm orb} + f_t$ measures the orbital energy of the bulge-bulge system when the bulges "touch." η can be decomposed into two separate parts, with one contribution from the initial orbital energy at large radii ($f_{\rm orb}$) and the other from the subsequent energy transfer between the stellar bulges and dark matter halos during the merger (f_t); see BMQ for more details. The values of f and η for our equal-mass merger simulations are listed in Table 2. These results show that, as argued in the previous paragraph, at fixed initial orbital energy (fixed $f_{\rm orb}$), increasing the orbital angular momentum results in a larger value of η, which is due to more energy transfer from the bulges to the halos (a larger positive value of f_t). This in turn leads to a more tightly bound remnant bulge with a larger σ and smaller R_e (Fig. 3).

We can gain an analytical understanding of Fig. 3 and Table 2 by investigating how α in the $R_e - M_*$ relation varies with the energy and structural parameters η and f in equation (7). Assuming that the stellar mass doubles in equal-mass mergers (i.e. $M_{*,f} = 2M_{*,i}$, a very good approximation to the simulations) and that the stellar effective radius scales as $R_e \propto M_*^{\alpha}$ upon merging, equation (7) relates the exponent α to η and f:

$$\alpha = 1 - \frac{\ln(1 + \eta/4f_i)}{\ln 2} + \frac{\ln(f_f/f_i)}{\ln 2}\,. \tag{9}$$

We therefore expect $\alpha = 1$ if a merger is on a parabolic orbit with negligible energy transfer ($\eta = f_{orb} + f_t = 0$) and unchanged structural parameters ($f_f = f_i$). By contrast, if the merger orbit initially has significant angular momentum (at distances $\gg R_i$), the bulges will spiral

TABLE 2
ENERGETICS

Run[a]	r_p[b]	f_{orb}	η ($\equiv f_t + f_{orb}$)	f_i	f_f
P1	0	0	0.225	0.367	0.521
P2	2.29	0	0.366	0.367	0.493
P3	12.5	0	0.451	0.367	0.494
P4	37.8	0	0.531	0.367	0.480
B1	0	0.145	0.275	0.367	0.513
B2	2.29	0.145	0.461	0.367	0.497
B3	20.8	0.145	0.539	0.367	0.488
B4	37.8	0.145	0.609	0.367	0.456
B5	57.1	0.145	0.619	0.367	0.433
B6	78.4	0.145	0.617	0.367	0.423

[a]Name of run
[b]Pericentric distance of orbit (kpc)

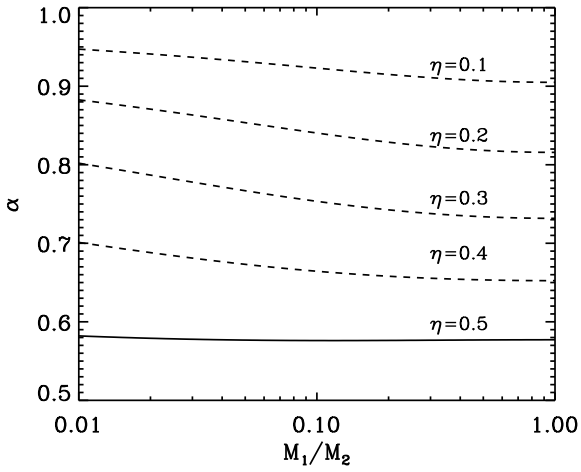

FIG. 4.— Logarithmic slope α of the stellar mass-size relation as a function of the mass ratio of the merging galaxies M_1/M_2 calculated from the analytical energy conservation model assuming $f_f = f_i$. Head-on (parabolic) mergers correspond to $\eta \approx 0$ while circular orbits have $\eta \approx 0.5$. The trend of increasing α with decreasing orbital angular momentum shown in Fig. 3 for our simulations is reproduced in this model, although we do not expect the values of α to match exactly due to simplifying assumptions made in the model (e.g. $f_f = f_i$). The dependence of α on the mass ratio is very weak, suggesting that the major merger results of Fig. 3 are also applicable to minor mergers. This is also confirmed by the similarities between our 1:1 and 0.33:1 simulations.

inward and dynamical friction will tend to make the orbits circular at small radii; in this case, $\eta \approx 0.5$ by the virial theorem and $\alpha \approx 0.58$ if $f_f = f_i$. In the actual simulations, Table 2 shows there is always nonzero energy transfer from stars to dark matter (i.e. $f_t > 0$), which decreases α for the head-on orbits, whereas the merged bulge always has a larger structural parameter (i.e. $f_f/f_i > 1$), which increases α. Together the variations in η and f explain the behavior and range of α (~ 0.7 to 1.3) shown in Fig. 3.

The fact that $f_f > f_i$ (by up to $\sim 40\%$) reflects the varying central dark matter content of the remnants, though in general it is non-trivial to quantitatively relate f_f/f_i to the change in dark matter fraction within R_e because equation (8) involves a radial integral over the stellar density profile and dynamical mass. However, from equation (8), we see that for a given distribution of stars (fixed R_e and ρ_*), increasing the amount of dark matter inside the bulge (i.e. increasing M_{dyn}) increases f_f, which is why $f_f > f_i$ in the simulations.

The analytical energy conservation model given in equations (7) and (9) can easily be extended to unequal mass mergers. Fig. 4 shows the general dependence of α on the mass ratio of the merging bulges for different values of η, assuming for simplicity parabolic orbits and $f_f = f_i$. As argued above, η is expected to decrease from ≈ 0.5 for orbits with substantial angular momentum to ≈ 0 for nearly parabolic head-on orbits. Correspondingly, α increases from ≈ 0.58 to 1. This trend of increasing α with decreasing orbital circularity (or r_{peri}) is consistent with that shown in Fig. 3 for the simulations, although we do not expect the values of α in the model and simulations to match exactly due to simplifying assumptions made in the model (e.g. $f_f = f_i$). Fig. 4 also shows that the dependence of α on the mass ratio M_1/M_2 is quite weak for $0.01 \leq M_1/M_2 \leq 1.0$, indicating that the results in Fig. 3 can be extended to very minor mergers. This analytic result is consistent with the fact that our 0.33:1 mergers and equal mass mergers show a similar dependence of α and β on merger orbit.

4. DISCUSSION AND IMPLICATIONS

4.1. *The Fundamental Plane and its Projections*

The results of Section 3.1 show that the fundamental plane is preserved during dissipationless mergers for a wide range of orbits, a result of virial equilibrium with a slight tilt due to an increasing central dark matter fraction. On the other hand, the results of Section 3.2 show that the projections of the fundamental plane are quite sensitive to the amount of energy transferred from the bulges to the dark matter halos during the merger, which is determined in large part by the merger orbit. If gas-poor mergers build up the massive end of the red sequence, as several current observations and models suggest, then our results indicate that the projections of the fundamental plane – but not necessarily the plane itself – provide a powerful way of investigating the assembly history of massive elliptical galaxies.

While a sample of 43 BCGs has been reported to lie on the fundamental plane (Oegerle & Hoessel 1991), they appear to have different fundamental plane projections from those of lower-mass elliptical galaxies. The correlation between effective radius and luminosity is steeper for these BCGs ($R_e \propto L^{1.25}$) than for all early-type galaxies ($R_e \propto L^{0.6}$) and the BCG velocity dispersions lie substantially lower than the extrapolation of the Faber-Jackson relation to higher luminosity (Oegerle & Hoessel 1991). Other properties of BCGs are notably different from those of normal ellipticals as well, such as their high incidence of secondary nuclei (Schneider et al. 1983), their more prolate shapes (Ryden et al. 1993), the small dispersion in their luminosities (Postman & Lauer 1995), and the large and relatively constant (out to $z \sim 0.4$) luminosity gap between BCGs and second-ranked cluster galaxies (Loh & Strauss 2005).

The results presented in this paper suggest that these differences are all signatures of how massive elliptical

galaxies were assembled. In particular, dissipationless merging of elliptical galaxies provides a natural mechanism for steepening both the Faber-Jackson and $R-L$ relations *and* preserving the overall fundamental plane, *provided that merger orbits become preferentially more radial for the most massive galaxies* (Fig. 3).

There is, in fact, support for this possibility in the literature. Observationally, it is well-established that BCGs are aligned both with their host clusters and the surrounding large scale structure (e.g. Binggeli 1982; Fuller et al. 1999; West & Blakeslee 2000). Numerical simulations show that anisotropic merging is natural in CDM models (Dubinski 1998; Zentner et al. 2005) and preferentially radial merging along filaments can produce many of the observed properties of clusters and BCGs (West 1994; West et al. 1995; Dubinski 1998). These lines of reasoning favor radial mergers during BCG formation and point to a strong connection between the characteristics of the mergers that form BCGs and the origin of observed BCG properties (and the differences between BCGs and normal ellipticals). In addition, the most luminous ellipticals in the Virgo cluster *all* seem to lie on a filament (West & Blakeslee 2000), which likely means that anisotropic merging is also important for luminous ellipticals that are not BCGs.

According to our calculations, projections of the fundamental plane provide independent information about the assembly history of massive ellipticals. Analysis of a large spectroscopic sample of massive galaxies would provide significantly stronger constraints on changes in the fundamental plane projections at the highest masses; we expect that the indications of deviations seen in current samples will become more apparent with additional data.

4.2. *Supermassive black holes*

Any departure from the canonical Faber-Jackson relation in massive galaxies would also have significant implications for the demography of supermassive black holes. In particular, under the assumption that black holes coalesce following a gas-poor merger (which is not guaranteed; see, Merritt & Milosavljevic 2004 for a review), the black hole mass should increase roughly in proportion to the galaxy mass since the amount of mass-energy carried away in gravitational waves is likely to be quite small (e.g., Baker et al. 2004). We therefore expect that dissipationless mergers will maintain a linear $M_{\rm BH}-M_*$ relation. Any steepening of the $L-\sigma_c$ relation for luminous ellipticals, however, should then be reflected in a corresponding steepening in the $M_{\rm BH}-\sigma$ relation for massive black holes. Wyithe (2005) has argued that just such a steepening is present in the current sample of black hole masses, but the statistics are rather poor and a larger sample is needed in order to make definitive statements. If correct, black hole masses for very luminous galaxies based on the canonical $M_{\rm BH}-\sigma_e$ relation (Gebhardt et al. 2000; Ferrarese & Merritt 2000; Tremaine et al. 2002) would systematically underpredict the true black hole mass (see also Lauer et al. 2006, in prep.).

4.3. *Further discussions*

Several issues can be investigated in more detail to test our suggestion that preferential radial merging is responsible for many of the morphological and kinematical properties of BCGs. One promising possibility is to study the shapes of BCGs. Porter et al. (1991) find that the outer regions of BCGs are generally prolate, with the inner regions being rounder. Ryden et al. (1993) find that the distribution of BCG ellipticities has a similar mean value to that of all ellipticals but with a smaller dispersion and a tendency to be slightly more prolate. For comparison, we find that the remnants of 1:1 mergers on low-L orbits are quite prolate with a tendency toward triaxiality: generally a:b:$c\sim$ 1.8:1:1. By contrast, in the runs with significant angular momentum, a:b:$c\sim$ 1.7:1.3:1. However, the main difference between our equal mass and 0.33:1 mergers is that the 0.33:1 remnants are notably rounder than their 1:1 counterparts, an effect also seen by Villumsen (1982). Unequal mass major mergers thus lead to the same overall trends we see in the fundamental plane and its projections while producing more spherical remnants. Using shapes to quantitatively test the predictions of our models will thus require detailed information about the orbits and mass ratios of the mergers that formed BCGs.

The above considerations highlight the need to move beyond non-cosmological major merger simulations of spherical and isotropic galaxies that have been the focus of this paper as well as many earlier papers. Indeed, the relaxation and virialization of a cluster generally involves several massive galaxies with a range of masses (Dubinski 1998). In addition, the shapes of cluster-mass dark matter halos in dark matter-only cosmological simulations are typically quite prolate at formation but then become rounder (but still triaxial) as time goes on (Hopkins et al. 2005; Allgood et al. 2005) due to a transition from filamentary to spherical accretion (Allgood et al. 2005). Clearly, high resolution two-component (stars and dark matter) simulations in a cosmological context with full formation histories are necessary for making detailed predictions about the properties of massive ellipticals. We are currently working on such simulations. Although we expect that our basic conclusions about the fundamental plane and its projections will remain unchanged, repeated major and minor merging on realistic cosmological orbits will significantly influence the shapes and kinematics of the remnant galaxies.

As one final implication of the non-spherical nature of our merger remnants, we note that the measured velocity dispersion can change by more than 15% with viewing angle for a given remnant. For the most massive galaxies, this could be significant: a galaxy that has $\sigma_e\approx 350$ km/s from most viewing angles (typical for a BCG) could have $\sigma_e > 400$ km/s in certain rare configurations (we find that the observed velocity dispersion is $\approx$ 15% higher than the mode $\approx$ 3% of the time for the remnants of relatively radial mergers). This viewing angle effect would be a source of scatter in the $M_{\rm BH}-\sigma_e$ and Faber-Jackson relations. In addition, our results imply that there should be a population of massive ellipticals with anomalously large velocity dispersions and small radii for their luminosity. These objects would be prolate merger remnants viewed down the major axis. Bernardi et al. (2005) have recently reported the detection of a population of luminous galaxies with these properties. A simple test of our explanation for these galaxies is to look at their projected shapes: our calculations predict these

galaxies should appear statistically rounder than other galaxies of comparable luminosity.

We thank Sandy Faber, Zoltan Haiman, and Tod Lauer for useful discussions and Volker Springel for making GADGET publicly available. This work used resources from the NERSC, which is supported by the US DOE. C-PM is supported in part by NSF grant AST 0407351 and NASA grant NAG5-12173. EQ is supported in part by NSF grant AST 0206006, NASA grants NAG5-12043 and ATP05-54, an Alfred P. Sloan Fellowship, and the David and Lucile Packard Foundation.

REFERENCES

Allgood, B., Flores, R. A., Primack, J. R., Kravtsov, A. V., Wechsler, R. H., Faltenbacher, A., & Bullock, J. S. 2005, astro-ph/0508497
Baker, J., Campanelli, M., Lousto, C. O., & Takahashi, R. 2004, Phys. Rev. D, 69, 027505
Bell, E. F., et al. 2005, astro-ph/0506425
Bell, E. F., et al. 2004, ApJ, 608, 752
Bender, R., Burstein, D., & Faber, S. M. 1992, ApJ, 399, 462
Benson, A. J. 2005, MNRAS, 358, 551
Bernardi, M., et al. 2003a, AJ, 125, 1866
—. 2003b, AJ, 125, 1849
Bernardi, M., et al. 2005, astro-ph/0510696
Binggeli, B. 1982, A&A, 107, 338
Binney, J., & Tremaine, S. 1987, Galactic Dynamics (Princeton, NJ, Princeton University Press, 1987)
Blanton, M. R. 2005, astro-ph/0512127
Blumenthal, G. R., Faber, S. M., Flores, R., & Primack, J. R. 1986, ApJ, 301, 27
Boylan-Kolchin, M., Ma, C.-P., & Quataert, E. 2005, MNRAS, 362, 184
Capelato, H. V., de Carvalho, R. R., & Carlberg, R. G. 1995, ApJ, 451, 525
Ciotti, L., Lanzoni, B., & Renzini, A. 1996, MNRAS, 282, 1
De Lucia, G., Springel, V., White, S. D. M., Croton, D., & Kauffmann, G. 2005, astro-ph/0509725
Djorgovski, S., & Davis, M. 1987, ApJ, 313, 59
Dressler, A., Lynden-Bell, D., Burstein, D., Davies, R. L., Faber, S. M., Terlevich, R., & Wegner, G. 1987, ApJ, 313, 42
Dubinski, J. 1998, ApJ, 502, 141
Faber, S. M., Dressler, A., Davies, R. L., Burstein, D., & Lynden-Bell, D. 1987, in Nearly Normal Galaxies: From the Planck Time to the Present, 175–183
Faber, S. M., & Jackson, R. E. 1976, ApJ, 204, 668
Faber, S. M., et al. 1997, AJ, 114, 1771
Faber, S. M., et al. 2005, astro-ph/0506044
Ferrarese, L., & Merritt, D. 2000, ApJ, 539, L9
Fuller, T. M., West, M. J., & Bridges, T. J. 1999, ApJ, 519, 22
Gebhardt, K., et al. 2000, ApJ, 539, L13
Gerhard, O., Kronawitter, A., Saglia, R. P., & Bender, R. 2001, AJ, 121, 1936
Gnedin, O. Y., Kravtsov, A. V., Klypin, A. A., & Nagai, D. 2004, ApJ, 616, 16
González-García, A. C., & van Albada, T. S. 2003, MNRAS, 342, L36
Hernquist, L. 1990, ApJ, 356, 359
Hopkins, P. F., Bahcall, N. A., & Bode, P. 2005, ApJ, 618, 1
Jorgensen, I., Franx, M., & Kjaergaard, P. 1996, MNRAS, 280, 167
Kauffmann, G., & Haehnelt, M. 2000, MNRAS, 311, 576
Kazantzidis, S., Magorrian, J., & Moore, B. 2004, ApJ, 601, 37
Khochfar, S., & Burkert, A. 2003a, astro-ph/0309611
—. 2003b, ApJ, 597, L117
Kormendy, J., & Bender, R. 1996, ApJ, 464, L119
Loh, Y.-S., & Strauss, M. A. 2005, astro-ph/0510500
McIntosh, D. H., et al. 2005, ApJ, 632, 191
Merritt, D. 1985, ApJ, 289, 18
Merritt, D., & Milosavljevic, M. 2004, astro-ph/0410364
Naab, T., Khochfar, S., & Burkert, A. 2005, astro-ph/0509667
Navarro, J. F., Frenk, C. S., & White, S. D. M. 1997, ApJ, 490, 493
Nipoti, C., Londrillo, P., & Ciotti, L. 2003, MNRAS, 342, 501
Oegerle, W. R., & Hoessel, J. G. 1991, ApJ, 375, 15
Padmanabhan, N., et al. 2004, New Astronomy, 9, 329
Pahre, M. A., de Carvalho, R. R., & Djorgovski, S. G. 1998a, AJ, 116, 1606
Pahre, M. A., Djorgovski, S. G., & de Carvalho, R. R. 1998b, AJ, 116, 1591
Porter, A. C., Schneider, D. P., & Hoessel, J. G. 1991, AJ, 101, 1561
Postman, M., & Lauer, T. R. 1995, ApJ, 440, 28
Robertson, B., Cox, T. J., Hernquist, L., Franx, M., Hopkins, P. F., Martini, P., & Springel, V. 2005, astro-ph/0511053
Ryden, B. S., Lauer, T. R., & Postman, M. 1993, ApJ, 410, 515
Schneider, D. P., Gunn, J. E., & Hoessel, J. G. 1983, ApJ, 264, 337
Shen, S., Mo, H. J., White, S. D. M., Blanton, M. R., Kauffmann, G., Voges, W., Brinkmann, J., & Csabai, I. 2003, MNRAS, 343, 978
Springel, V., Yoshida, N., & White, S. D. M. 2001, New Astronomy, 6, 79
Tran, K.-V. H., van Dokkum, P., Franx, M., Illingworth, G. D., Kelson, D. D., & Schreiber, N. M. F. 2005, ApJ, 627, L25
Tremaine, S., et al. 2002, ApJ, 574, 740
Trujillo, I., Burkert, A., & Bell, E. F. 2004, ApJ, 600, L39
van Dokkum, P. G. 2005, AJ, 130, 2647
van Dokkum, P. G., Franx, M., Fabricant, D., Kelson, D. D., & Illingworth, G. D. 1999, ApJ, 520, L95
Villumsen, J. V. 1982, MNRAS, 199, 493
West, M. J. 1994, MNRAS, 268, 79
West, M. J., & Blakeslee, J. P. 2000, ApJ, 543, L27
West, M. J., Jones, C., & Forman, W. 1995, ApJ, 451, L5
Wyithe, S. 2005, astro-ph/0503435
Zentner, A. R., Kravtsov, A. V., Gnedin, O. Y., & Klypin, A. A. 2005, ApJ, 629, 219